Ekoloji 27(106): 113-121 (2018)

N80 Oil Tube Steel Corrosion Behavior in Different CO_2 Saturated Brine

Yun Ma [1,2*], Qingbo Zhang [2], Haitao Bai [3]

[1] College of Petroleum Engineering, Xi'an Shiyou University, Xi'an 710065, CHINA

[2] Key Laboratory of Environment Pollution Control Technology of Oil Gas and Reservior Protection, Xi'an Shiyou University, Xi'an 710065, CHINA

[3] Southwest Petroleum University, Chengdu 610500, P.R. CHINA

* Corresponding author: mayun9401@xsyu.edu.cn

Abstract

The experiment was carried out to illustrate the corrosion behavior of N80 exposed to CO_2-saturated brine conditions through electrochemical experiments, corrosion mass loss methods and surface analysis. With the increase of the CO_2 pressures and temperatures, the corrosion product films were gradually thicken but non-uniform. The corrosion products on the sample surface were crystalline and/or amorphous structures, mainly composed of $FeCO_3$. With the increase of CO_2 pressures at 50 °C, the corrosion rate would gradually experience three stages, and when the CO_2 pressure was 2MPa, the corrosion rate was up to the maximum value and the surface of sample had the characteristics of pit erosion and mesa corrosion. With the rise of temperatures at 10 MPa, the corrosion rates of N80 pipeline steel increased slowly from 65°C to 80°C because of the thicker corrosion products, but the pitting corrosion increased because the $FeCO_3$ and $CaCO_3$ would be amorphous structures.

Keywords: CO_2-saturated brine, corrosion rate, pitting, corrosion products

Ma Y, Zhang Q, Bai H (2018) N80 Oil Tube Steel Corrosion Behavior in Different CO_2 Saturated Brine. Ekoloji 27(106): 113-121.

INTRODUCTION

Carbon dioxide (CO_2) in the atmosphere continues to cause global climate change, which has brought serious economic losses to countries. In order to relieve CO_2 pollution, many researchers countered CO_2 capture and storage (CCS) and CO_2 enhanced oil recovery (CO_2-EOR). The process of CCS involves three stages: capture of the CO_2 from the power plant or industrial process, transmission of the CO_2, and its subsequent storage into a geological reservoir. Among them, CO_2-EOR is the most economical way because it increases the profitability of the oil filed (Bi et al. 2011, Cole et al. 2011, Gale and Davison 2004, Stevens 2003, Xiang et al. 2012).

However, in the process of implementing CO_2-EOR, there were some problems. Among them, the CO_2 corrosion of equipment and pipeline affect the safety, economic and environmental benefits of CO_2-EOR. The frequent corrosion and pitting of oil well casing and leakage of CO_2 scrap resulted in the failure of CO_2-EOR, and even caused catastrophic accidents and serious environmental pollution (Halseid et al. 2014, Lu et al. 2002, Yan et al. 2012).

The recent understanding was mainly focus on the majority of the pipelines on the extreme environment, such as J55, P110, N80 for high pressure service. Pure CO_2 was essentially non-corrosion to carbon steel, but carbonic acid would be formed once a free water phase was present. A few papers gave general and excellent description (theoretical and experimental) of various conditions to explain CO_2 corrosion. For example, corrosion rate could be influenced by a layer of corrosion products formed on steel surfaces. The corrosion layers and protective properties always determined a long-term corrosion performance (Chen et al. 2002, Cui et al. 2006, Gao et al. 2011, Haleem et al. 2014, Lotz et al. 1991, Wu et al. 2013, Zhang et al. 2012). But few papers gave the relationships between corrosion rate, pitting condition and the characters of corrosion products, which is very important and necessary.

Based on the investigation described above, the objective of this work is to systematically investigating the N80 oil tube steel corrosion in different CO_2 saturated brine oil tube steel behaviors through electrochemical experiments and dynamic corrosion tests. The macro-morphology of corrosion layer was

© Foundation Environmental Protection & Research-FEPR Received: 29 May 2018 / Accepted: 10 Sep 2018

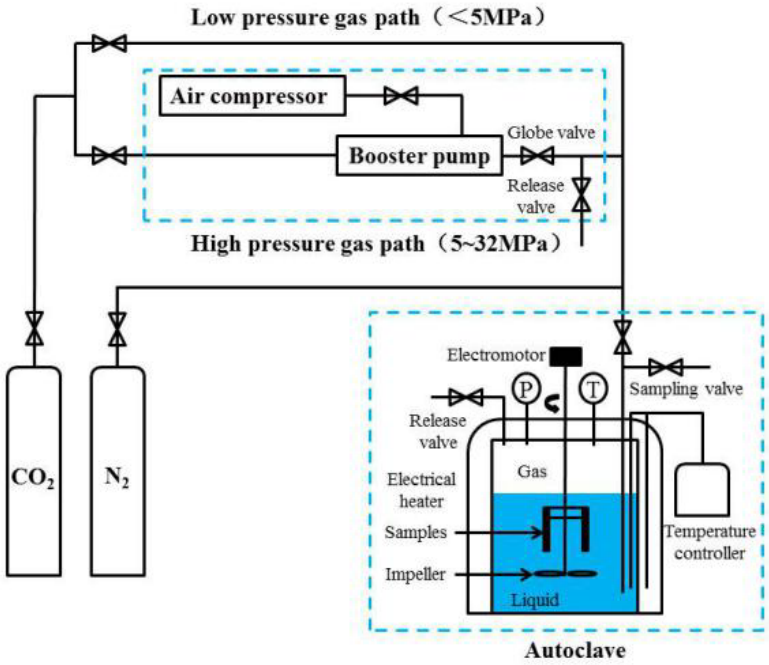

Fig. 1. Self-built CO_2 corrosion resistant performance evaluation system

studies by a camera, and the micro-morphology of corrosion layer was observed with scanning electron microscope (SEM) and optical microscope (OM). The chemical composition was observed by energy dispersive spectroscope (EDS) and X-ray Diffraction (XRD). Through the above studies and analysis, it could be explained that the relationships between corrosion rate, pitting condition and the characters of corrosion products.

MATERIALS AND EXPERIMENTS

The test solution used in the study contained 44.8553g/L NaCl, 33.2940g/L $CaCl_2$,1.4295g/L $MgCl_2$, 0.2440g/L Na_2SO_4 and $NaHCO_3$ 0.063g/L. The specimens for corrosion tests were machined with 50mm×13mm×1.5mm and the specimens for electrochemical measurements were sectioned into working electrode (area, 0.785cm^2), exhibiting nominal compositions as follows (mass%), C:0.33, Si:0.28, Mn:1.19, P:0.020, Cr:0.013, Ni:0.026, Mo:0.016, Ti:0.020 and Fe balance. The model steel was provided by the China research institute. The corrosion coupons were cleaned with petroleum ether and ethanol, stove-dried, weighted and stored in a vacuum desiccator before carrying out any surface analysis experiments. To make an electrical connection, it was necessary to weld a thread to the sample as the working electrode. The samples were embedded in epoxy coating and left one surface to be exposed to the electrolyte. After mechanical grinding (until 1200 grit SiC paper), the samples were cleaned in ultrasonic ethanol before experiments (Zhang et al. 2017).

CO_2 corrosion behavior was evaluated with the self-built CO_2 corrosion resistant performance evaluation system (CCRPES, **Fig. 1**). Among them, the dynamic autoclave (Parr-4578) was made by Parr company (USA). The specimens were immersed for the duration of 48h after putting into the CO_2 saturated Brine. Before corrosion test, the solution was deoxygenated with pure nitrogen for 2h using purified N_2.

Three specimens were used for each corrosion test. Among three specimens for each duration, two specimens were used for corrosion mass loss measurement. After corrosion scale was removed using the chemical cleaning procedure, the specimens were rinsed by distilled water, then dried and finally reweighed by the electronic analytical balance with an accuracy of 0.1 mg to calculate the average corrosion rate. In this work, the corrosion rate of the tested samples is defined as the corrosion depth per year, i. e. mm/a (Lot 2013). The last one was used for surface observation. The morphology of corrosion layer was studies using a camera (D810, NiKon, Japan), and the microphology of corrosion layer was observed SEM (Quantu 600FEG, USA). The 3D morphology of the corroded samples was surveyed with OM (Opto-digital DSX-500, Olympus, Japan). The chemical composition was observed by EDS (OXFORD INCA x-act, UK) and XRD (D/MAX-2400, Japan)

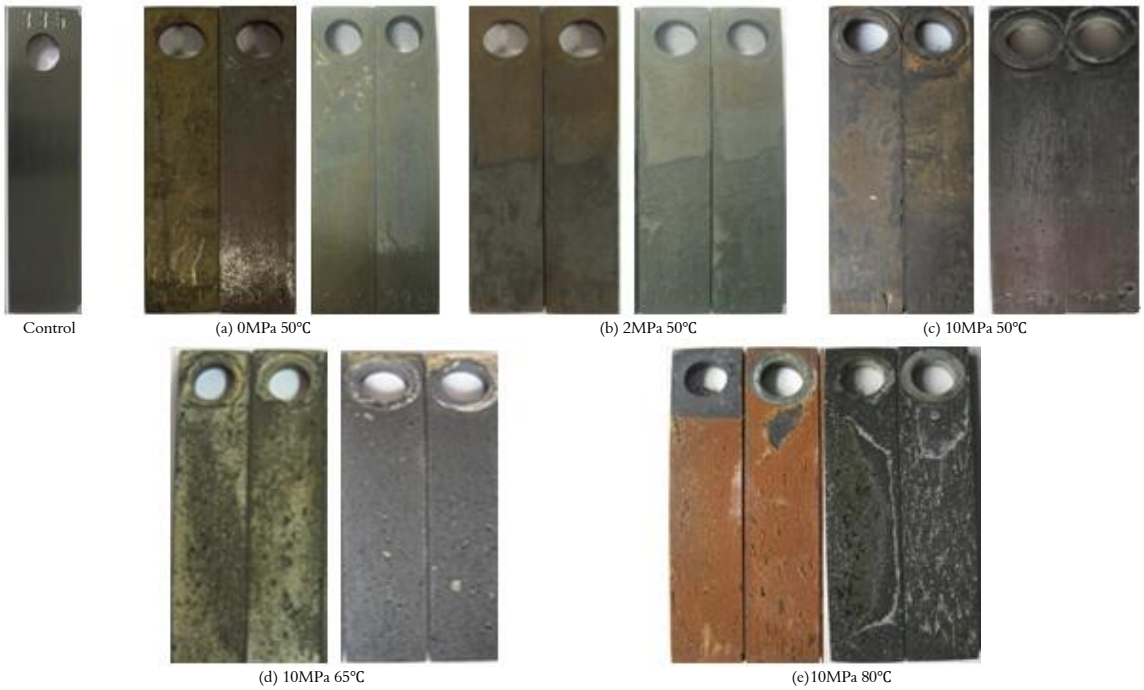

Fig. 2. Corrosion product film morphology of corroded samples at difference CO_2 pressures and temperatures

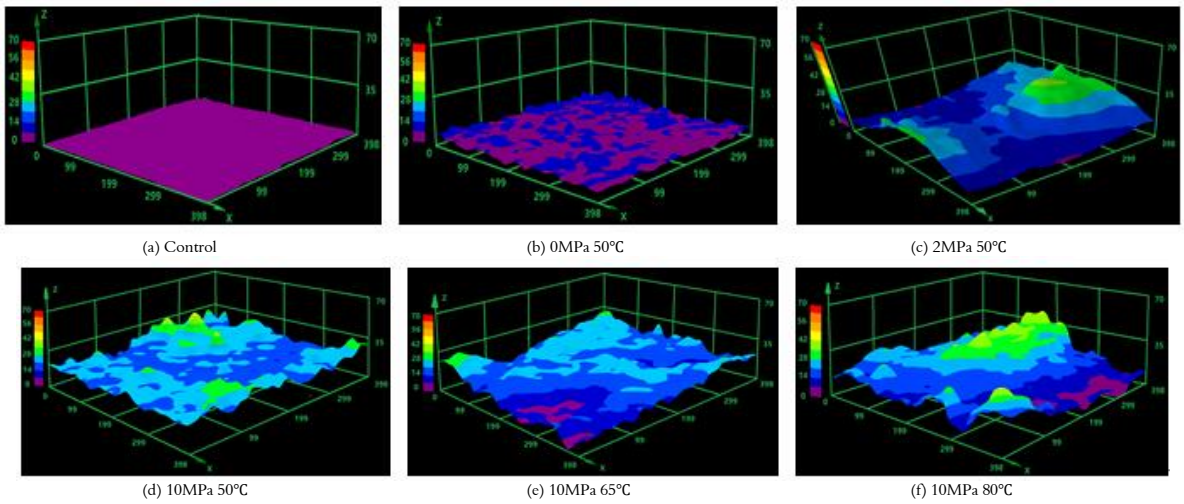

Fig. 3. Map of OMU Pond I and sampling station (Anonymous 1975)

The specimens under different conditions were carried out to analyze by electrochemical measurement (ParStat-2273, USA). The tests were performed using a three-electrode system. A graphite electrode was used as the auxiliary electrode. The saturated Ag/ AgCl was used as the reference electrode, and the test specimen was used as the working electrode. The glass electrolysis pool had a capacity of 500mL. Before the measurements, the test solution was deoxygenated for 2h using purified N_2. The electrochemical impedance spectroscopy (EIS) measurements were performed under potentiostatic conditions in a frequency range from 100 kHz to 0.01 Hz, with amplitude of 10 mV AC signal. All the measurements were carried out at open circuit potential. The experimental data were analyzed by using the commercial software ZsimpWin.

RESULTS AND DISCUSSIONS

Surface Condition

Fig. 2 showed the macroscopic morphologies of N80 steel before and after the removal of corrosion scaling products in CO_2 saturated brine environment with different CO_2 pressures and temperatures at a corrosion time of 48 h. **Fig. 3** showed the 3D morphology of the corroded samples at different CO_2 pressures and temperatures.

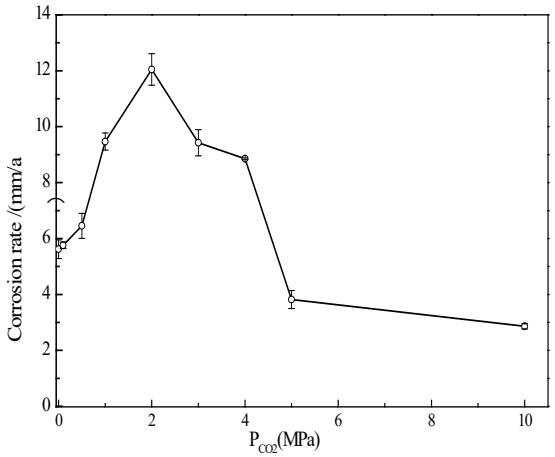

Fig. 4. Relationships between CO_2 pressures and corrosion rates at 50℃

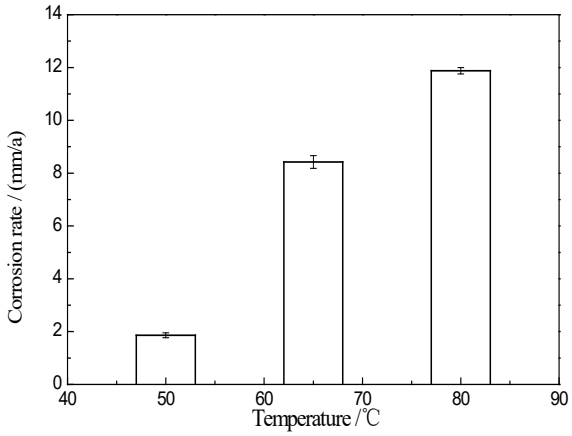

Fig. 5. Relationships between immersion temperatures and corrosion rates (10MPa)

The surface of the sample was covered with brown corrosion and scaling products. With the increase of the CO_2 pressures and temperatures, the corrosion product films were gradually more thicken. After the removal of corrosion scale, a slightly smooth matrix surface of steel could be observed.

When the CO_2 pressure was 2MPa, the surface of sample had the characteristics of pit erosion and mesa corrosion (**Fig. 2b** and **Fig. 3**). It could be clarified with a Mesa Attack Corrosion (Nyborg 1998). When the CO_2 pressure was 10MPa, the pitting corrosion could be clearly seen on the surface of corroded samples (**Fig. 2c**). Wang YaFei reported a phenomenon, which the mild steel had certain pitting tendency, and the pits were formed by mechanical defects and metal inclusions and metal-ion accumulation on the interface of corrosion products (Gao et al. 2014, Wang et al. 2016).

When the temperature was 80℃, obvious pitting has been seen on the surface, which indicated that the corrosion pattern has gradually developed to pitting corrosion with the thickening of the corrosion product film (**Fig. 2**). The reason for this phenomenon was that the salinity of the system was high, and there are a lot of Ca^{2+} and Mg^{2+}. The influence on the formation of the corrosion product film and the adhesion force on the surface were complicated (Zhang et al. 2017). Once the corrosion product film was thinner than others, or it's adhesion force was smaller than others, the pitting formed.

Average Corrosion Rate

Fig. 4 and **5** showed the relationships between the corrosion rates with CO_2 pressures and the temperatures of the tested sample in saturated with CO_2 for 48h. When CO_2 pressure increased from 0~2MPa, corrosion rate increased from 5.6188mm/a to 12.0446mm/a. But when the pressure increased from 2 to 10MPa, the corrosion rate decreased to 2.8606mm/a. When the CO_2 pressure was 2MPa, the corrosion rate was up to the maximum value. Generally speaking, dry CO_2 was not corrosive. However, the general amount of CO_2 dissolved into water, and the presence of CO_2 in solution resulted in the formation of carbonic acid (the equation was $CO_2+H_2O=H_2CO_3$), which promoted the progress of CO_2 corrosion reaction (Cui et al. 2004). Due to the increasing of CO_2 pressures, the solubility of CO_2 in solution increased, which leaded that the acidity of solution was strengthened. Ultimately, the corrosion rate could increases. But with the increasing of CO_2 pressures, the decrease of CO_2 corrosion rates was mainly resulted from the passivation of the surface by corrosion layer formed on the steels. With the increasing solubility of $[CO_3^{2-}]^{\star}[Fe^{2+}]$, the corrosion product film deposition was accelerated, which are benefit to the formation of corrosion product film. Corresponding to corrosion product film of the specimens was shown in **Fig. 2** and **Fig. 6**.

The corrosion rates increased sharply while the temperature was up to the range of 50~65℃, and the increasing of corrosion rate tended to be gentle at 65 ~80℃. The ablation rate of Fe in the solution increased as the temperature increases, which resulted in that corrosion reaction rate could be accelerated. However, when the temperature increased from 65℃ to 80℃, the corrosion rate increased slowly. On the one hand, the solubility of CO_2 decreased in liquid phase. On the other hand, due to the corrosion product film was formed on the surface of the matrix, the contact area would hinder the substrate and corrosion medium, the

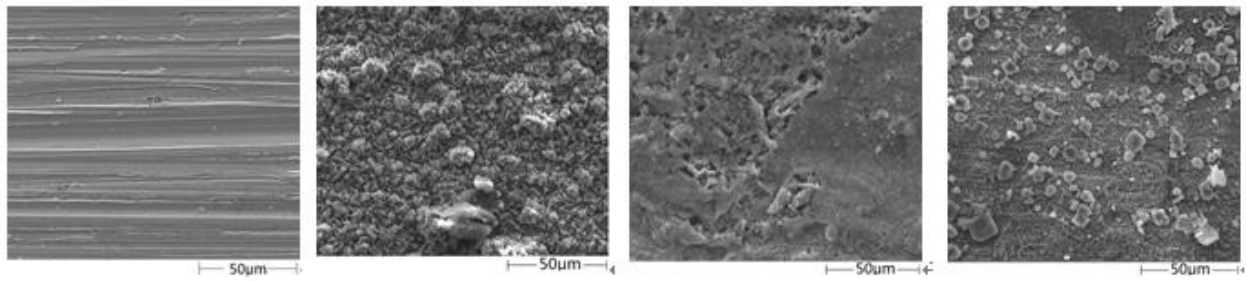

(a)Control (b) 0MPa (c) 2MPa (d)10MPa

Fig. 6. SEM images of corroded surface of N80 samples N80 for 48h at different CO_2 pressures(×2000)

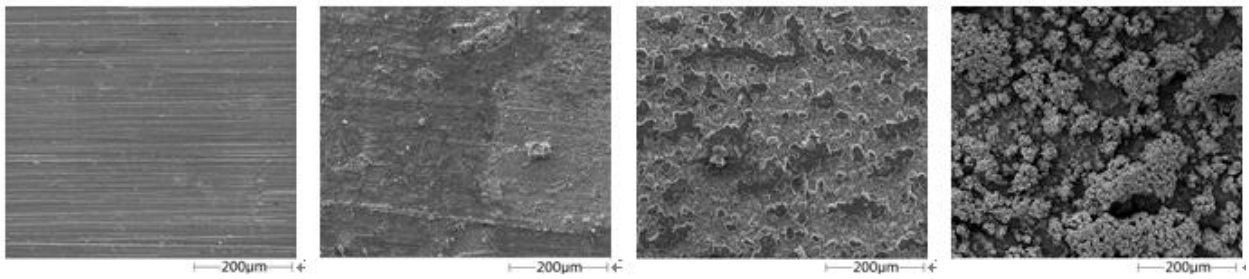

(a)Control (a)50℃ (b)65℃ (c)80℃

Fig. 7. SEM images of corroded surface of N80 samples N80 for 48h at different CO_2 pressures(×2000)

corrosion rate increased slowly (Cui et al. 2004, 2006). Corresponding to corrosion product film of the specimens was shown in **Fig. 2** and **Fig. 7**.

Corrosion Film Structure

SEM analysis

Fig. 6 showed the surface morphologies of the corroded samples for 48h at different CO_2 pressures. The SEM images revealed that corrosion film were so roughness and not compact that easily peeled off at lower CO_2 pressures. Liu et al improved the number of micro-defects increased gradually at lower pressures ((Liu et al.2015)). The white crystal may be scaling and corrosion products. At the CO_2 pressure was 0MPa, the corrosion products on the matrix was easy to fall off. The corrosion process would be improved (**Fig. 6b**). At the CO_2 pressure was 2MPa, it was seen that more pores existed on the surface of corrosion product film. The solution easily contacted with matrix to promote CO_2 corrosion (**Fig. 6c**). When the CO_2 pressure increased from 2 to 10MPa, the corrosion product film became more compact (**Fig. 6d**), which leaded to the changing tendency of corrosion rates as shown in **Fig. 4**.

Fig. 7 show the SEM images of surface of corroded samples for 48h at different temperatures. When the temperature was less than 65 °C, the molecular energy enlarged with the increase of temperature, which could result in the increase of the contact probability of ions and steel surface. Meanwhile, the formed corrosion products were loose and unstable, and then fell off naturally. Therefore, the corrosion rate would increase. It was obviously that the products formed at 80℃ looked thicker and non-uniform than that formed at 50℃ or 65℃, which would behave as a good diffusion barrier to prevent the underlying steel from further dissolution. Therefore, the corrosion rate would moderately increase when the reaction temperature was higher than 65℃ (Cui et al. 2004, 2006, Gao et al. 2014, Liu et al. 2014, 2016), and the changing tendency of corrosion rates (**Fig. 5**), which should lead to the pitting corrosion.

EDS and XRD analysis

The composition of CO_2 corrosion scale formed at various temperatures and different pressures under CO_2 saturated Brine conditions as shown in **Fig. 8**, and **Table 1** shows the EDS Element analysis of N80 samples surface at various temperatures and different pressures under CO_2 saturated Brine conditions. The results of EDS indicated that the composition of CO_2 corrosion scales were not the same at various conditions, but the main elements in the CO_2 corrosion scale were all Fe, O and C. Based on the XRD and EDS results (**Fig. 9**), these crystal layers were predominately $FeCO_3$ along with some peaks related to solid solution of Ca(Fe, Mg)CO_3 and a very few $CaCO_3$. When the temperature was 80℃ and the CO_2 pressure was 10 MPa, these crystal layers were predominately Ca(Fe, Mg)CO_3, but the $FeCO_3$ and $CaCO_3$ would be amorphous structures, which looked more thicker but less uniform than that formed at 50℃ or 65℃ (**Fig. 7**).

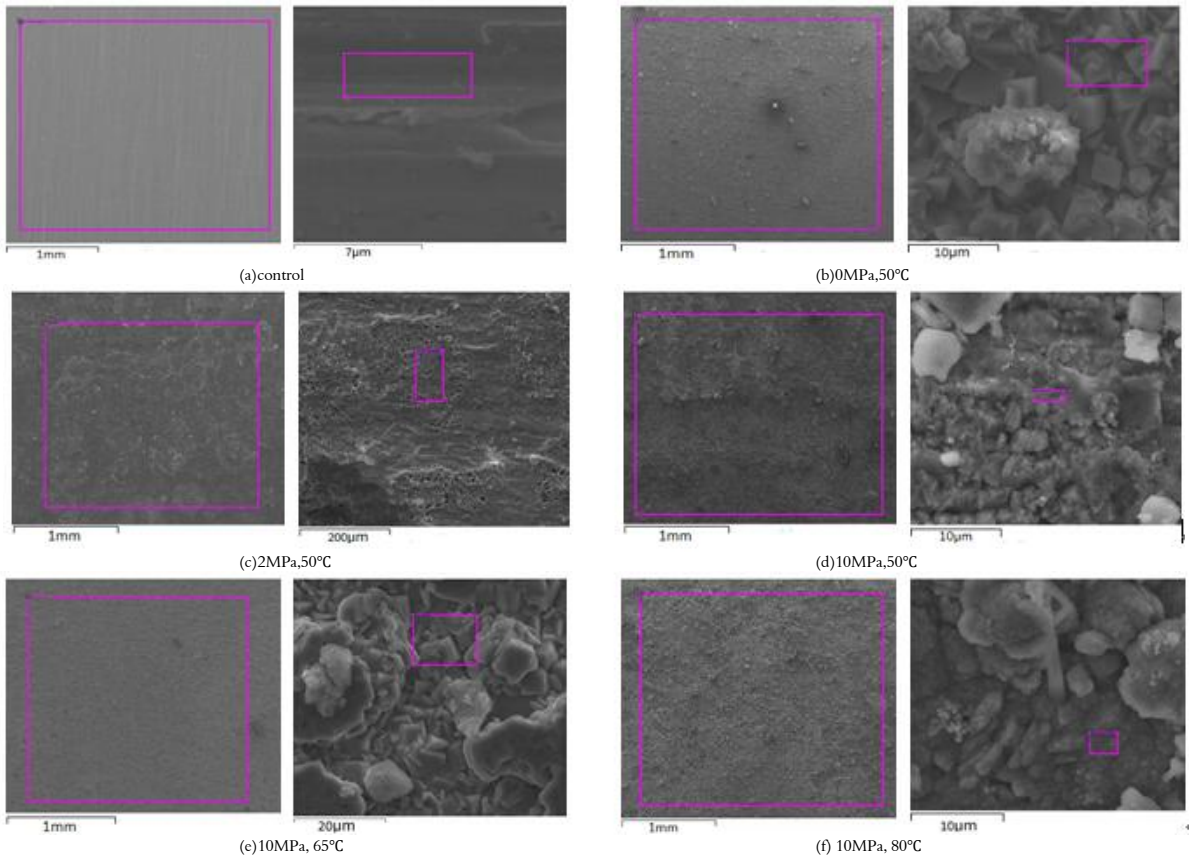

Fig. 8. EDS of N80 coupon surface at difference CO_2 partial pressures or temperature

Table 1. EDS element analysis of N80 samples surface at different condition (atom.%)

Condition and view		Element								Total
		C K	O K	Na K	Si K	Cl K	Ca K	Mn K	Fe K	
Control	Big view	/	/	/	0.19	/	/	1.80	98.01	100
	Small view	/	/	/	0.21	/	/	1.89	97.9	
0MPa,50℃	Big view	23.66	59.21	0.31	0.03	0.06	0.78	/	15.95	
	Small view	16.36	59.09	/	/	0.1	1.19	0.45	22.81	
2 MPa,50℃	Big view	21.01	49.24	4.35	/	1.46	5.16	0.43	18.35	
	Small view	20.48	41.47	3.50	/	1.17	1.58	3.85	27.95	
10 MPa,50℃	Big view	17.10	48.27	2.79	0.51	12.1	1.40	0.43	17.40	
	Small view	21.27	64.73	/	/	0.88	0.54	/	12.58	
10 MPa,65℃	Big view	19.23	48.36	4.80	0.03	4.49	1.47	/	21.62	
	Small view	30.64	50.19	3.07	/	2.7	1.04	/	12.37	
10 MPa,80℃	Big view	21.41	54.31	2.07	/	1.17	5.11	0.26	15.32	
	Small view	15.72	56.48	/	/	0.49	7.83	0.48	18.98	

When the content of crystal corrosion products decreased, the corrosion rate increased. Meanwhile, the content of amorphous corrosion products was dominated, the corrosion rate increased slowly or even fell, but the pitting increased quickly because of the characters of amorphous corrosion products, such as loose, thicker and less uniform than crystal corrosion products (**Fig. 2** and **Fig. 3**).

EIS Measurements

Based on the investigation, it has been proved that the corrosion rates of steels in CO_2 environments depend on the formation of $FeCO_3$ scale and their protective characteristics. To further explore the different characteristics of $FeCO_3$ corrosion product scales formed at different temperatures, EIS (Bai et al. 2006, Cao and Zhang 2002, Mansfeld 1990, Wei et al. 2015) is used to evaluate the corrosion resistance of coatings. It was shown in **Fig. 10** that the EIS plots of N80 steel in CO_2 saturated Brine solution at different temperatures. A similar characteristic was observed among the Nyquist plots - a capacitive reactance arc (Mansfeld 1990, Yan et al. 2012). The capacitive arc radius was further reduced, and polarization resistance conditions was gradually decreased as the temperature increased, and the corrosion rate increased satisfied with the changing tendency of corrosion rates as shown in **Fig. 5**. According to Nyquist and Bode -|P|, it could be seen that there were one time constant in the whole frequency range when the corrosion temperature

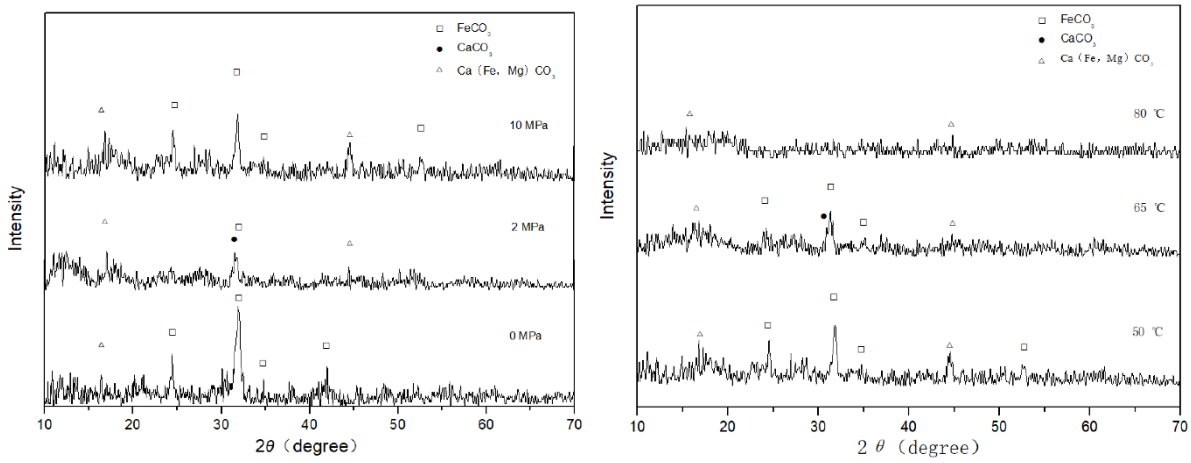

(a) Different CO_2 pressure (50℃) (b) Different temperature (10MPa)

Fig. 9. XRD of N80 coupon surface at difference CO_2 partial pressures or temperature

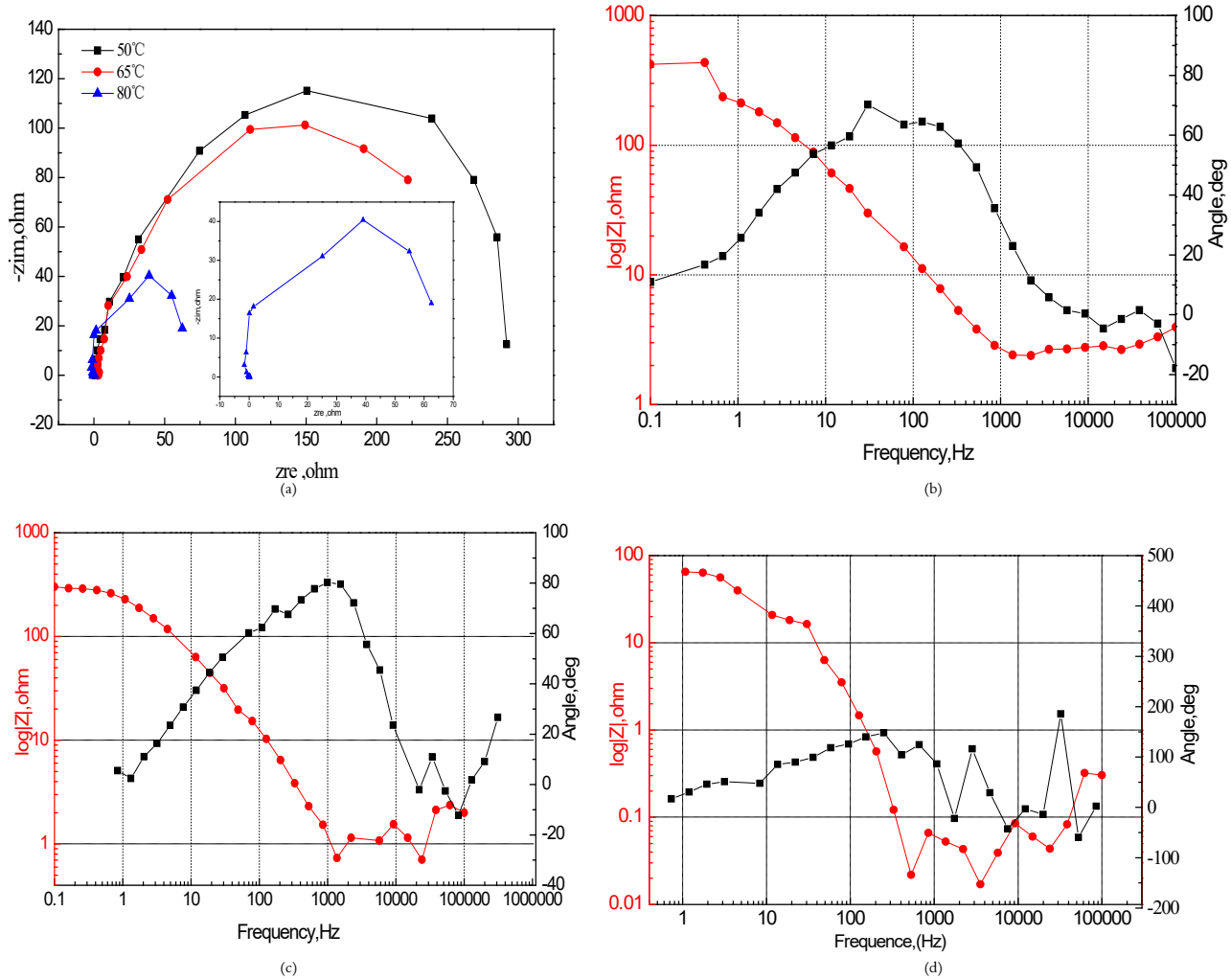

Fig. 10. The EIS plots of corrosion of N80 steel in CO_2 saturated solution at different temperatures:(a) the nyquist plots at different temperatures; (b)the Bode plots at 50℃, (c)the Bode plots at 65℃ and (d) the Bode plots at 80℃

increased from 50 to 80℃, and Bode-|Z| showed that low frequency impedance value decreased, which indicated that the corrosive medium had started the specimen surface and leaded to serious pitting corrosion (as shown in **Fig. 2a**, **2b**). When the temperature was 80℃, Bode-|Z| showed that low frequency impedance value decreased one order of magnitude between 100 and 1000 ohm.

CONCLUSION

As the CO_2 pressure increase from 0 to 10MPa at 50℃, the change of corrosion rate would gradually experience three stages: rapid rise stage, slow decline stage and the smooth invariant stage. When the CO_2 pressure was 2MPa, the corrosion rate was up to the maximum value and the surface of sample had the characteristics of pit erosion and mesa corrosion. As the CO_2 temperature increase from 50 to 80℃ at 10MPa, the change of corrosion rate would gradually experience two stages: rapid rise stage and slow rise stage. The corrosion products on the sample surface were crystalline and/or amorphous structure, mainly composed of C, O, and Fe, which were composed of $FeCO_3$. The corrosion rate and pitting condition had relations with the characters of corrosion product films. When the content of crystal corrosion products decreased, the corrosion rate increased. However, the content of amorphous corrosion products is dominated, the corrosion rate increased slowly or even fall, but the pitting increased quickly because of the characters of amorphous corrosion products, such as loose, thicker and less uniform than crystal corrosion products.

ACKNOWLEDGEMENTS

The authors are grateful for financial support from National Natural Science Foundation of China (51504193) and Key laboratory Research Project of Shaanxi Education Department (15JS090).

REFERENCES

Bai ZQ, Chen CF, Lu MX (2006) Analysis of EIS characteristics of CO_2 corrosion of well tube steels with corrosion scales. Applied Surface Science, 252: 7578-7584. https://doi.org/10.1016/j.apsusc.2005.09.011

Bi FQ, Li F, Liang H (2011) Domestic and foreign research and application progress on CO2-EOR technology. Value Engineering, 30: 206-207.

Cao CN, Zhang JQ (2002) Introduction of electrochemical impedance spectroscopy, Beijing science press, Beijing.

Chen CF, Lu MX, Zhao GX (2002) Characters of corrosion scales on well tube steel N80. Acta metallurgica sinice, 38: 411-416.

Cole IS, Corrigan P, Sim S (2011) Corrosion of pipelines used for CO_2 transport in CCS: is it a real problem? International Journal of Greenhouse Gas Control, 5: 749–756. https://doi.org/10.1016/j.ijggc.2011.05.010

Cui ZD, Wu SL, Li CF (2004) Corrosion behavior of oil tube steels under conditions of multiphase flow saturated with super-critical carbon dioxide. Materials letters, 58: 1035-1040. https://doi.org/10.1016/j.matlet.2003.08.013

Cui ZD, Wu SL, Zhu SL (2006) Study on corrosion properties of pipelines in stimulated produced water saturated with super-critical CO_2. Applied surface science, 252: 2368- 2374. https://doi.org/10.1016/j.apsusc.2005.04.008

Gale J, Davison J (2004) Transmission of CO_2-safety and economic considerations. Energy, 29: 1319-1328. https://doi.org/10.1016/j.energy.2004.03.090

Gao CL, Liu ML, Li DP (2014) Effects of CO_2 partial pressure on CO_2 corrosion behavior of N80 tubular steel. Corrosion & Protection, 35: 975-978.

Gao M, Pang X, Gao K (2011) The growth mechanism of CO_2 corrosion product films. Corrosion Science, 53: 557–568. https://doi.org/10.1016/j.corsci.2010.09.060

Haleem SAME, Wanees SAE, Bahgat A (2014) Environmental factors affecting the corrosion behaviour of reinforcing steel. VI. Benzotriazole and its derivatives as corrosion inhibitors of steel. Corrosion Science, 87: 321-333. https://doi.org/10.1016/j.corsci.2014.06.043

Halseid M, Dugstad A, Morland B (2014) Corrosion and bulk phase reactions in CO_2 transport pipelines with impurities: review of recent published studies. Energy Procedia, 63: 2557-2569. https://doi.org/10.1016/j.egypro.2014.11.278

Liu QY, Mao LJ, Zhou SW (2014) Effects of chloride content on CO_2 corrosion of carbon steel in simulated oil and gas well environments. Corrosion Science, 84: 165–171. https://doi.org/10.1016/j.corsci.2014.03.025

Liu ZG, Gao XH, Li JP (2016) Corrosion behavior of low-alloy martensite steel exposed to vapour-saturated CO_2 and CO_2-saturated brine conditions. Electrochimica Acta, 213: 842-855. https://doi.org/10.1016/j.electacta.2016.08.024

Lot RT (2013) Pitting corrosion evaluation of austenitic stainless steel type 304 in acid chloride media. Journal of Materials Environmental Science, 4: 448-459.

Lotz U, van Bodegom L, Ouwehand C (1991) The effect of type of oil or gas condensate on carbanic acid corrosion. Corrosion, 48: 635-645. https://doi.org/10.5006/1.3585301

Lu MX, Bai ZQ, Zhao X (2002) Actuality and typical cases for corrosion in the process of extraction, gathering, storage and transmission for oil and gas. Corrosion protect, 23: 105-113.

Mansfeld F (1990) Electrochemical impedance spectroscopy as a new tool for investigating methods of corrosion protection. Electrochimica Acta, 35: 1533-1544. https://doi.org/10.1016/0013-4686(90)80007-B

Nyborg R (1998) Initiation and growth of mesa corrosion attack during CO2, Corrosion of Carbon Steel. Corrosion/98, Paper no 48, NACE.

Stevens SH (2003) Storage of CO_2 in depleted oil and gas fields: global capacity, costs and barriers, Colling wood, AU: CSIRO Publishing, Victoria.

Wang YF, Cheng GX, Li Y (2016) Observation of the pitting corrosion and uniform corrosion for X80 steel in 3.5Wt.%NaCl solutions using in-situ and 3-D measuring microscope. Corrosion Science, 111: 508-517. https://doi.org/10.1016/j.corsci.2016.05.037

Wei L, Pang XL, Liu C (2015) Formation mechanism and protective property of corrosion product scale on X70 steel under supercritical CO2 environment. Corrosion Science, 100: 404–420. https://doi.org/10.1016/j.corsci.2015.08.016

Wu Q, Zhang Z, Dong X (2013) Corrosion behavior of low-alloy steel containing 1% chromium in CO_2 environments. Corrosion Science, 75: 400-408. https://doi.org/10.1016/j.corsci.2013.06.024

Xiang Y, Wang Z, Yang XX (2012) The upper limit of moisture content for supercritical CO_2 pipeline transport. Journal of Supercritical Fluids, 67: 14–21. https://doi.org/10.1016/j.supflu.2012.03.006

Yan W, Deng JG, Li XR (2012) Effects of silty sand on CO_2 corrosion behavior of low-Cr tubing steel. Science Bulletin, 57: 927-934. https://doi.org/10.1007/s11434-011-4947-4

Zhang GA, Liu D, Guo XP (2017) Corrosion behavior of N80 carbon steel in formation water under dynamic supercritical CO2 condition. Corrosion Science, 120: 107-120. https://doi.org/10.1016/j.corsci.2017.02.012

Zhang J, Wang ZL, Wang ZM (2012) Chemical analysis of the initial corrosion layer on pipeline steels in simulated CO_2-enhanced oil recovery brines. Corrosion Science, 65: 397-407. https://doi.org/10.1016/j.corsci.2012.08.045